Computers and Geosciences 109 (2017) 247–257

Contents lists available at ScienceDirect

Computers and Geosciences

journal homepage: www.elsevier.com/locate/cageo

Research paper

New spatial upscaling methods for multi-point measurements: From normal to p-normal

Feng Liu [a,c], Xin Li [a,b,c,*]

[a] Key Laboratory of Remote Sensing of Gansu Province, Northwest Institute of Eco-Environment and Resources, Chinese Academy of Sciences, Lanzhou 730000, China
[b] Chinese Academy of Sciences Center for Excellence in Tibetan Plateau Earth Sciences, Beijing 100101, China
[c] University of Chinese Academy of Sciences, Beijing 100049, China

ARTICLE INFO

Keywords:
Generalized Gaussian distribution
Multi-scale
Least power estimation
Geostatistics
Soil moisture
Heihe Watershed Allied Telemetry Experimental Research (HiWATER)

ABSTRACT

Careful attention must be given to determining whether the geophysical variables of interest are normally distributed, since the assumption of a normal distribution may not accurately reflect the probability distribution of some variables. As a generalization of the normal distribution, the p-normal distribution and its corresponding maximum likelihood estimation (the least power estimation, LPE) were introduced in upscaling methods for multi-point measurements. Six methods, including three normal-based methods, i.e., arithmetic average, least square estimation, block kriging, and three p-normal-based methods, i.e., LPE, geostatistics LPE and inverse distance weighted LPE are compared in two types of experiments: a synthetic experiment to evaluate the performance of the upscaling methods in terms of accuracy, stability and robustness, and a real-world experiment to produce real-world upscaling estimates using soil moisture data obtained from multi-scale observations. The results show that the p-normal-based methods produced lower mean absolute errors and outperformed the other techniques due to their universality and robustness. We conclude that introducing appropriate statistical parameters into an upscaling strategy can substantially improve the estimation, especially if the raw measurements are disorganized; however, further investigation is required to determine which parameter is the most effective among variance, spatial correlation information and parameter *p*.

1. Introduction

The multi-scale problem indicates that the scale-dependent variation in a geophysical variable should be considered when observing or estimating the value of that variable at diverse scales. This problem has received significant attention (Atkinson and Tate, 2000; Famiglietti et al., 2008; Gruber et al., 2013; Mandelbrot, 1967) and has become one of the most important challenges faced by scientists performing Earth observations and simulations because the multi-scale problem has a general impact on land surface data comparisons, assimilations, and so on. The multi-scale problem has once again emerged due to improvements in Earth observation and modeling technologies and the increase in geodata availability.

In general, multi-scale problems in geoscience stem from the fact that the relationships between geophysical variables at different scales are highly non-linear. This non-linearity is mainly caused by the representativeness issue of observations or simulations. That is, one can only detect the "truth" of a geophysical variable at a single support in space and time (Li, 2014), whereas most models simulate the dynamic processes at a certain scale, with reduced performance at other scales. This non-linearity is also caused by the lack of some physical information. For example, this issue arises when using a numerical operator to replace an ideal model or enforcing the use of traditional 2-point statistics to address the connectivity patterns (Meerschman et al., 2013; Renard and Allard, 2013). Therefore, if the measurement scale differs from that of a model (Li, 2014; Vereecken et al., 2007; Wang et al., 2004), data comparison or transformation from one scale to another scale must be performed, thereby possibly introducing significant uncertainties into the modeling process.

One can address this problem using upscaling methods, which consider the transformation of heterogeneous land surface characteristics at fine scales to homogeneous characteristics at larger scales (Atkinson and Tate, 2000; Vereecken et al., 2007). There are three main types of transformation processes in upscaling methods, i.e., dynamic process

* Corresponding author. Key Laboratory of Remote Sensing of Gansu Province, Northwest Institute of Eco-Environment and Resources, Chinese Academy of Sciences, Lanzhou 730000, China.
E-mail addresses: liufeng@lzb.ac.cn (F. Liu), lixin@lzb.ac.cn (X. Li).

http://dx.doi.org/10.1016/j.cageo.2017.08.001
Received 10 November 2016; Received in revised form 6 July 2017; Accepted 1 August 2017
Available online 2 August 2017

upscaling (Vereecken et al., 2007), statistical upscaling (Atkinson and Tate, 2000) and mixed upscaling (combining the first two). Dynamic process upscaling methods focus on modeling the physical phenomena across different scales, and partial differential equations are generally formulated in this process. The upscaling methods in this study, unless otherwise indicated, are only related to statistical upscaling. This study does not include dynamic process upscaling methods or mixed methods. One of the easiest methods involves directly regarding a single-point measurement as a large-scale "truth". However, this method produces large errors because point measurements simply represent the state of the geophysical variable at its own support. If these types of data are directly converted to the desired scale, they will not maintain their original spatial representativeness (Atkinson and Tate, 2000; Woodcock and Strahler, 1987) and will not sufficiently represent the true value of a geophysical variable at the large-scale. Other methods, such as the weighted spatial average of multi-point measurements, can effectively improve the upscaling results. Based on this concept, various in situ observation networks (Gruber et al., 2013; Jin et al., 2014; Molotch and Bales, 2005) have recently been launched. Meanwhile, the demand for advanced upscaling methods continues to gradually increase.

Generally, the assumption of a normal distribution is not enough to represent the statistics of a geophysical variable of interest. Among the commonly used upscaling methods, statistical algorithms based on the best linear unbiased estimator (BLUE) are generally accepted. In these types of algorithms, various statistical parameters, such as the variance and spatial correlation, are used to construct the unbiased condition. Unfortunately, these methods are strongly dependent on the condition that the geophysical variable of interest is normally distributed (Chen et al., 1994). However, because uncertainty exists everywhere in the real world, it is difficult to obtain a precisely normal distribution. For example, parametric uncertainties can result in a non-normal distribution (Kitanidis, 1986). Even if strict quality control has been applied and the true distribution of a geographical element is normal, measurements, which can be considered samples of this distribution, are nearly normal but not strictly normal. Furthermore, if outliers are present in the data, the normal distribution-based methods may be very inaccurate, because they are used to find the maximum likelihood estimates by minimizing the least square error. These methods are less robust than some methods, such as those based on minimizing the least absolute error (Nyquist, 1980; Pennecchi and Callegaro, 2006). For example, a previous experiment (Wang et al., 2004) showed that the averaging method produces substantial deviations when the sample is non-normal.

Consequently, although the normal distribution assumption can be used to construct a simple and fast algorithm, this type of method will most likely result in a significant difference between the estimate and the "truth" because the geophysical variables of interest are not always strictly normal. This deficiency has motivated the development of a more reasonable statistical method to evaluate the relationships between measurements at different scales. As an extension of the normal distribution, the p-normal distribution (also known as generalized Gaussian distribution) and its best linear unbiased estimation, the least power estimation (LPE), have been studied (Money et al., 1982; Nyquist, 1980; Pennecchi and Callegaro, 2006; Pascal et al., 2013) and widely applied in fields such as signal processing (Chen et al., 1994; Krupiński and Purczyński, 2006; Kuruoğlu et al., 1998; Yarlagadda et al., 1985) and metrology (Pennecchi and Callegaro, 2006). This technique further provides an extra parameter (the shape parameter p) to handle more samples.

This study mainly addresses the following scientific issues. (1) How can new upscaling methods based on p-normal distributions be developed? (2) Do these methods perform better than classic methods? (3) What conclusions can we draw from the comparisons between the p-normal-based upscaling methods and the normal-based methods?

This paper is organized as follows. Chapter 2 presents the construction of a spatial model with correlation information and the development of the corresponding upscaling algorithms for multi-point measurements based on the concepts of p-normal distributions and LPE. In chapter 3, six upscaling methods are used in two experiments to test their performances using various types of data. Finally, these upscaling methods are discussed, and conclusions are presented.

2. Upscaling strategy

Generally, one can assume that an upscaling strategy can be expressed as follows:

$x^t = f_{up}(X^o) + \varepsilon$, where x^t is the "truth" of the geophysical variable of interest at a larger scale, $f_{up}(\cdot)$ is the upscaling method, $X^o = \{x_i^o | i = 1, \cdots, n\}$ represents a column vector comprised of simultaneous multi-point measurements, and ε is error. Due to the multi-dimensional measurement X^o, $f_{up}(\cdot)$ is based on the assumption that the geophysical variable of interest features either a multivariate normal or a multivariate non-normal distribution. However, as stated in the Introduction, it is unreasonable to consider the measurements normally distributed.

2.1. p-Normal distribution

The normal distribution consists of two parameters (the location and scale parameter, or mean and variance). Therefore, its probability density function (PDF) includes only a few parameters and fails to explain other samples in which the concentrations of values around the mean are different from that of a normal distribution. Compared to the normal distribution, the p-normal distribution, also known as the generalized Gaussian distribution (Krupiński and Purczyński, 2006), is better suited to a wider range of samples. The standard formula of a univariate p-normal distribution is as follows:

$$\varphi(x^o) = p\tau \Big/ 2\sigma\Gamma\left(\frac{1}{p}\right) exp\left(-\left[\frac{\tau}{\sigma}|x^o - x^t|^p\right]\right), \tau = \sqrt{\Gamma\left(\frac{3}{p}\right)\Big/\Gamma\left(\frac{1}{p}\right)}, \quad (1)$$

where x^t, σ and $\Gamma(\cdot)$ are the available measurements, standard deviation and Gamma function, respectively, and p is an additional parameter that creates a new degree of freedom for the PDF. Therefore the p-normal distribution can be regarded as a generalization of the normal distribution. If $p = 1$, $p = 2$ or $p \to \infty$, the samples are distributed according to a Laplace, normal or uniform distribution, respectively.

The relationship between p and kurtosis is significant: a large p is associated with high-precision measurements with small sample errors, whereas a small p is associated with a peaked and heavy-tailed sample distribution (Nyquist, 1980). An empirical formula (Money et al., 1982) was correspondingly introduced to estimate p:

$$p = 9/\widehat{k}^2 + 1, \quad (2)$$

where the sample kurtosis $\widehat{k}$ is $\widehat{k} = [m\sum_{j=1}^{m}(x_j^o - \overline{x}^o)^4]/[\sum_{j=1}^{m}(x_j^o - \overline{x}^o)^2]^2$ (Pennecchi and Callegaro, 2006) and m, x_j^o and $\overline{x}^o$ represent the amount of data, the measurements at time j and the average value of the measurements, respectively. Generally, the geophysical variable of interest can be characterized as having distributions between normal and very non-normal; thus, $1 \le p \le 2$ (Pennecchi and Callegaro, 2006).

2.2. Least power estimation

Generally, each type of distribution is associated with a corresponding maximum likelihood estimation method. For example, the estimation method for normal distributions is the least square estimation (LSE). Similarly, the maximum likelihood estimation for a p-normal distribution is LPE.

The simplest estimation equation is as follows:

$$X^o = BX^t + V, \quad (3)$$

which means that the available measurements X^o are the estimates of the "truth" $X^t = (x_1^t, x_2^t, \cdots, x_n^t)^T$, where $B = diag(\beta_i)$ and $V = \{v_i\}, i = 1, 2, \cdots, n$ represent the estimation coefficient matrix and estimation error vector, respectively. Based on Equation (1), the joint PDF of all available measurements is as follows:

$$\varphi = \prod_{i=1}^{n} \varphi_i(x_i^o) = \frac{\prod_{i=1}^{n} p_i \tau_i}{2^n \prod_{i=1}^{n} \sigma_i \Gamma\left(\frac{1}{p_i}\right)} exp\left(- \sum_{i=1}^{n} \left[\frac{\tau_i}{\sigma_i} \left| x_i^o - \beta_i x^t \right| \right]^{p_i} \right), \quad i = 1, \cdots, n \tag{4}$$

where $\tau_i = \sqrt{\Gamma\left(\frac{3}{p_i}\right) \Big/ \Gamma\left(\frac{1}{p_i}\right)}$. Equation (4) can be regarded as multivariate generalized Gaussian distribution (Pascal et al., 2013) assuming that each element of the measurement vector is observed independently. This assumption results that the scatter matrix in multivariate generalized Gaussian distribution is an identity matrix. However, it does not mean that there is no spatial correlation between the measurements. The missing spatial correlation will be compensated by a geostatistical strategy in the next section.

Note that σ_i, p_i and τ_i are known, so obtaining the maximum of φ is equivalent to finding the minimum of the following likelihood function:

$$L = \sum_{i=1}^{n} \left[\frac{\tau_i}{\sigma_i} \left| x_i^o - \beta_i \hat{x} \right| \right]^{p_i} = \sum_{i=1}^{n} \left[\frac{\tau_i}{\sigma_i} |v_i| \right]^{p_i}, \tag{5}$$

where the "truth" x^t is replaced by a large-scale estimate $\hat{x}$, and the error $v_i = x_i^o - \beta_i \hat{x}$. Setting $\partial L / \partial \hat{x} = 0, q_i = \tau_i / \sigma_i$ and $sgn(v_i) = \begin{cases} 1, & v_i > 0 \\ 0, & v_i = 0 \\ -1, & v_i < 0 \end{cases}$ yields the following:

$$\partial L / \partial \hat{x} = \sum_{i=1}^{n} \beta_i q_i^{p_i} p_i |v_i|^{p_i - 1} sgn(v_i) = \sum_{i=1}^{n} \beta_i q_i^{p_i} p_i |v_i|^{p_i - 2} v_i = 0. \tag{6}$$

If the error weight matrix is defined as $W = diag(q_i^{p_i} p_i |v_i|^{p_i - 2}), i = 1, \cdots, n$, then the matrix form of Equation (6) yields $BWV = 0$. With regard to $V = X^o - B\hat{x}$, the estimation function is as follows:

$$\hat{x} = (B^T W B)^{-1} B W X^o. \tag{7}$$

Equation (7) introduces a promising way to estimate x^t using the statistical parameters of measurements and also presents a nonlinear least power problem, which is parameterized by its arguments B and W. To solve this problem requires assigning an initial value to $\hat{x}$ and iterative optimization, we consequently develop the LPE algorithm based on iteratively reweighted least squares (IRLS) (Kuruoğlu et al., 1998; Yarlagadda et al., 1985) as follows:

(I) Let $\hat{x}(0)$ be an arbitrary initial value (to quickly obtain the desired result, LSE is recommended).
(II) $v_i(j) = x_i^o - \beta_i \hat{x}(j)$
(III) $W(j) = diag(q_i^{p_i} p_i |v_i(j)|^{p_i - 2})$
(IV) $\hat{x}(j+1) = [B^T W(j) B]^{-1} [B^T W(j)] X^o$
(V) Stop the algorithm if $|\hat{x}(j) - \hat{x}(j-1)|$ is less than a sufficiently small positive number or j is larger than a maximum number of iterations, otherwise go to (II).

2.3. Spatially correlated LPE

According to the logic of BLUE, the estimate of a geophysical variable can be regarded as a weighted linear combination of multi-point measurements at different scales. Therefore we can assume that each point-scale measurement is a linear combination of other point-scale measurements and the truth of the geophysical parameter at the large scale. The ith point-scale measurement x_i^o is as follows:

$$x_i^o = \beta_{ii} x^t + \sum_{j \neq i} \beta_{ij} x_j^o + v_i = \beta_{ii} x^t + R_i + v_i, i = 1, \cdots, n, \tag{8}$$

where β_{ii} and β_{ij} are linear weights, and $R_i = \sum_{j \neq i} \beta_{ij} x_j^o$. This relationship can also be written in matrix form:

$$X^o = \begin{pmatrix} B & E \end{pmatrix} \begin{pmatrix} X^t \\ R \end{pmatrix} + V, \tag{9}$$

where $B = diag(\beta_{ii}), R = \{R_i\}$ is an n-dimensional vector, and E is the $n \times n$ identity matrix.

Compared to estimation Equation (3), Equations (8) and (9) imply that β_{ii} represents the linear spatial relationship between x_i^o and x^t, such that x_i^o can be considered as a measurement of x^t at the location of x_i^o, and β_{ij} represents the relationships between x_i^o and measurement x_j^o. β_{ii} also represents the degree of importance of the estimate x^t to x_i^o. Due to the heterogeneity of the region of interest, this degree is not only positively correlated to the spatial similarity between x_i^o and x^t but also negatively correlated to the similarities between x_i^o and other measurements. Therefore, the weights are associated with the heterogeneity of a geophysical variable, and this heterogeneity has a negative impact on the representativeness of point-scale measurements x_i^o.

A spatial estimation equation should take into account the correlation between measurements at different locations. Thus, we construct multi-scale spatial models based on two typical methods: geostatistics and inverse distance weighting (IDW). The former method mainly uses ordinary kriging, which is a typically generalized least square regression algorithm (Goovaerts, 1997) and can be regarded as the maximum likelihood estimator only if the measurements rely on the normality assumption, whereas the latter method does not depend on this assumption. Both are applied to the upscaling algorithms in this study and are abbreviated as GSLPE and IDWLPE.

According to geostatistics and Equation (8), the spatial model of GSLPE is as follows:

$$x_i^o = \lambda_{i,0} \hat{x} + R_i + v_i, \tag{10}$$

where $\beta_{ii} = \lambda_{i,0}$ and $\beta_{ij} = \lambda_{i,j}, j = 1, \cdots, i-1, i+1, \cdots, n$. The kriging weight vector $\lambda_i = (\lambda_{i,0}, \lambda_{i,1}, \cdots, \lambda_{i,i-1}, \lambda_{i,i+1}, \cdots, \lambda_{i,n})^T$ can be calculated using the equations of ordinary kriging (Goovaerts, 1997):

$$\begin{cases} \sum_{k=0, k \neq i}^{n} \lambda_{i,k} \gamma(c_j - c_k) - \xi = \gamma(c_j - c_i) \\ \sum_{k=0, k \neq i}^{n} \lambda_{i,k} = 1 \end{cases}, j = 0, 1, \cdots, i-1, i+1, \cdots, n \tag{11}$$

where ξ is the Lagrange multiplier, $\gamma(\cdot)$ is a semivariogram, c_i is the geographic location where x_i^o is measured, and c_0 is the geometrical center coordinate of the study area.

In Equation (10), β is replaced by the kriging weight vector λ, which is also a normalized weight with respect to the weights between x_i^o and other measurements. Here, the weight vector λ is collected in a different way from the regular kriging methods. According to Equation (8), which requires the true value x^t to be a component of x_i^o, we first assume the unknown estimate $\hat{x}$ is available and its geographic coordinate is the geometrical center coordinate of the study area c_0, then the ordinary kriging equation with respect to x_i^o is formulated by $\hat{x}$ and $x_j^o (j = 1, \cdots, i-1, i+1, \cdots, n)$, from which the desired kriging weight vector λ is obtained. Note that the unknown estimate $\hat{x}$ will not result in unsolved equations because the semivariograms associated with $\hat{x}$ are obtained by a fitting model (such as an exponential model) that was

formulated using all of the available measurements in advance.

Compared to the modeling of GSLPE, the spatial modeling of IDWLPE is much simpler. In Equation (8), let $\beta_{ii} = d_{i,0}/\sum_{j=0}^{n} d_{i,j}$ and $\beta_{ij} = d_{i,j}/\sum_{j=0}^{n} d_{i,j}$, where $d_{i,j}$ is the distance between geographic locations c_i and c_j.

Regarding the spatial estimation in Equation (8), Equations (5) and (7) can be extended as follows in Equations (12) and (13), respectively:

$$L = \sum_{i=1}^{n} \left[q_i \left| x_i^o - (\beta_{ii} \quad 1) \begin{pmatrix} \hat{x} \\ R_i \end{pmatrix} \right| \right]^{p_i} = \sum_{i=1}^{n} [q_i |v_i|]^{p_i}, \tag{12}$$

$$\hat{x} = (B^T W B)^{-1} (BW)(X^o - R). \tag{13}$$

Therefore, the GSLPE and IDWLPE algorithms are the same as the LPE, except that the iteration equation in step (IV) is changed to $\hat{x}(j+1) = [B^T W(j) B]^{-1} [B^T W(j)](X^o - R)$ according to Equation (13).

3. Experiments

3.1. Methods

The numerical experiments were designed to compare upscaling methods that are based on normal and non-normal distributions.

We adopted six methods: the multi-point arithmetic average (AA), LSE, block kriging (BK) (Goovaerts, 1997), LPE, GSLPE and IDWLPE. The first three methods can only obtain the corresponding maximum likelihood estimator based on normality. Among them, the spatial arithmetic average assumes that the upscaling estimator of the multi-point measurements is a mean. The LSE has been extended by weighting the different measurement variances in a linear combination equation, and BK provides a result by introducing the spatial correlation. These six algorithms focus on different combinations of statistical parameters, and their relationships are shown in Fig. 1.

In Fig. 1, four statistical parameters – location, scale, p and spatial correlation information – are listed, and the last three parameters are used to generate the three corresponding shaded circles. The overlapping regions of the shaded circles indicate that the method(s) in this region should consider the corresponding parameters. Thus, the arithmetic average simply focuses on the location parameter, the LSE algorithm focuses on the scale parameter, and BK algorithm focuses on the spatial correlation. Compared to the LSE, the LPE further introduces the p-normal distribution, and both the GSLPE and IDWLPE incorporate all four parameters.

3.2. Synthetic experiment

In the synthetic experiment, a spatial correlation region was established. This region was regularly discretized using 9 × 9 points (see Fig. 2), and a measurement was available at each point, except the red one at the center of the region. All of the available synthetic measurements were generated using a spatially correlated normal random field (generated by the geoR package, see: http://leg.ufpr.br/geoR/), of which the spatial mean, nugget, sill and range of the geostatistical semivariogram model were 10, 1, 2, and 10, respectively. Therefore, the study region is mean homogeneous, and the macro-scale true value of the region can be regarded as 10.

In the synthetic experiment, three numerical tests were conducted to evaluate the performances of each method.

(1) An accuracy test was used to identify the method that generated the best upscaling estimates. The criterion of this test is the mean absolute error (MAE), which is given as $\varepsilon_a = \frac{1}{m}\sum_{i=1}^{m} |\hat{x} - x^t|$, where m is the simulation time, and a smaller ε_a indicates a better performance.

(2) A stability test was used to calculate how well an upscaling method reacted to the diverse number of point measurements. Based on the accuracy test, s points ($s = 2, 3, \ldots, 80$), which were randomly selected from measurements at the same observation time, were upscaled using each method. The criterion of this test is the average MAE, which is given as $\overline{\varepsilon_a} = \frac{1}{N_r}\sum_{i=1}^{N_r} \varepsilon_a$, where N_r is the repeat time for each s.

(3) A robustness test was used to determine how well each upscaling method reacted to the point measurements with a given number of outliers. This test was also based on the accuracy test. Specifically, each measurement in the accuracy test was randomly amplified or minimized according to a particular probability, and the MAE values of these modified measurements were calculated.

3.3. Real-world experiment

A real-world experiment was performed using soil moisture data collected during an intensive observation period of the Heihe Watershed Allied Telemetry Experiment Research (HiWATER) project (Li et al., 2013) in 2012. The relevant study region is located in the 962 × 962 m^2

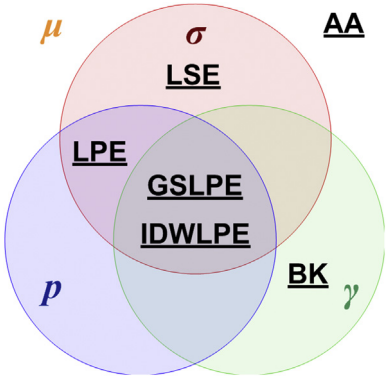

Fig. 1. The relationships with respect to four statistical parameters between the six upscaling methods. An overlapping region of shaded circles means all the involved parameters should be considered. (μ: location parameter, σ: scale parameter, p: p parameter, γ: spatial correlation information).

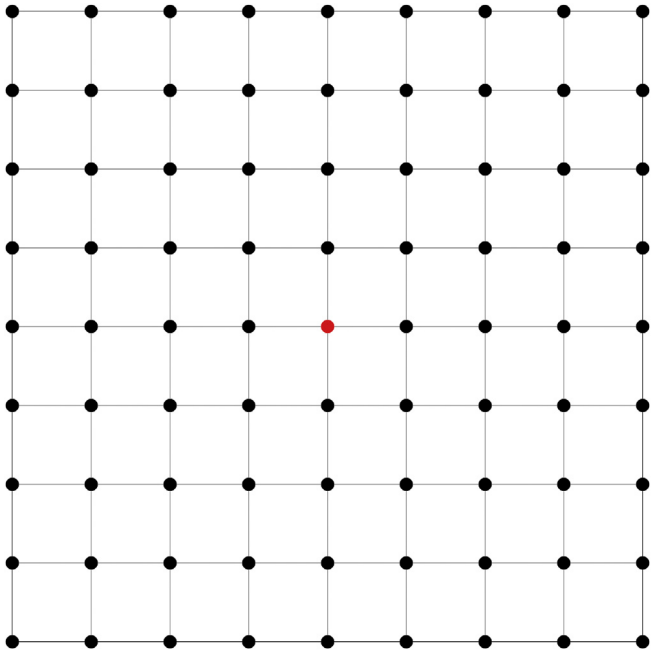

Fig. 2. The region of 9 × 9 simulated point-scale measurements for the synthetic experiment. All of the measurements were known except the red point at the center of the region. (For interpretation of the references to colour in this figure legend, the reader is referred to the web version of this article.)

Yingke-Daman irrigation district in the midstream region of the Heihe River Basin. Using eco-hydrological wireless sensor networks, a point-scale to footprint-scale observational network of soil elements was installed. Additional details of this project have previously been published (Jin et al., 2014; Li et al., 2013).

In the sensor networks, the point measurements were based on 10 WATERNET and 50 SoilNET sensors that simultaneously collected point-scale soil data at depths of 4 and 10 cm. The footprint -scale measurements were COsmic-ray Soil Moisture Observing System (COSMOS) observations. COSMOS provides footprint-scale soil moisture data collected at a maximum depth of 76 cm using a cosmic-ray fast neutron probe (Zhu et al., 2015). The collection frequency and spatially representative scale were 6 times per hour and 10 cm for the point measurements and once per hour and 700 m for the footprint measurements.

In the real-world experiment, all of the observational instruments were carefully quality controlled and calibrated (Jin et al., 2014; Zhu et al., 2015). We regarded the COSMOS data as the truth at a large scale and then upscaled the point-scale measurements using diverse upscaling methods.

To make the point and footprint measurements correspond to one another, appropriate data preprocessing techniques were applied. First, for equivalence with the COSMOS data in terms of both the collection frequency and observational depth, the hourly means of the point measurements at depths of 4 and 10 cm were vertically averaged. Second, the COSMOS data were retrieved by COSMIC (COsmic-ray Soil Moisture Interaction Code) modeling after smoothing the measured cosmic-ray neutron counts (Han et al., 2014).

There are 4 WATERNET and 20 SoilNET sensors at the scale of COSMOS that can be used to provide experimental data (Fig. 3). The vectors X^o and $C = \{c_i\}$, which can be used to construct the spatial model, are composed of hourly means and geographic coordinates of these 24 point measurements, respectively.

3.4. Estimation of parameters

Before the experiments, the corresponding statistical parameters of each point measurement dataset should be estimated. We use an empirical formulation of Equation (2) to estimate p: $p = \begin{cases} 2, & \widehat{k} < 3 \\ \frac{9}{\widehat{k}^2} + 1, & others \end{cases}$ because the p parameter ranges from 1 to 2 in real-world problems (Pennecchi and Callegaro, 2006).

In the synthetic experiment, the variance is $\sigma_i^2 = \frac{1}{m}\sum_{i=1}^{m}(x_i^o - \overline{x}^o)^2$, where i, m, x_i^o and $\overline{x}^o$ represent the ith point measurement, the amount of data, the observation at time i and the location parameter, respectively. In the real-world experiment, according to calibration accuracies, the observational precisions (variances) of the SoilNET and WATERNET sensors were 0.010 $m^3\ m^{-3}$ and 0.032 $m^3\ m^{-3}$, respectively.

3.5. Results

For the accuracy test of the synthetic experiment, at each simulated point, 1000 simulations were generated by 1000 random fields according to the location of the point. These 1000 random fields are independent identical distribution, i.e., they are generated by the same semivariogram model introduced in Section 3.2.

The frequency distributions of many geophysical variables feature sharper peaks and heavier tails than those of increments $\Delta x = x(d = |c_1 - c_2|) = x_1 - x_2$ when the distance d is small and that the opposite case is true when d increases (Panzeri et al., 2016; Riva et al., 2015). This phenomenon can be introduced as a criterion for determining whether a

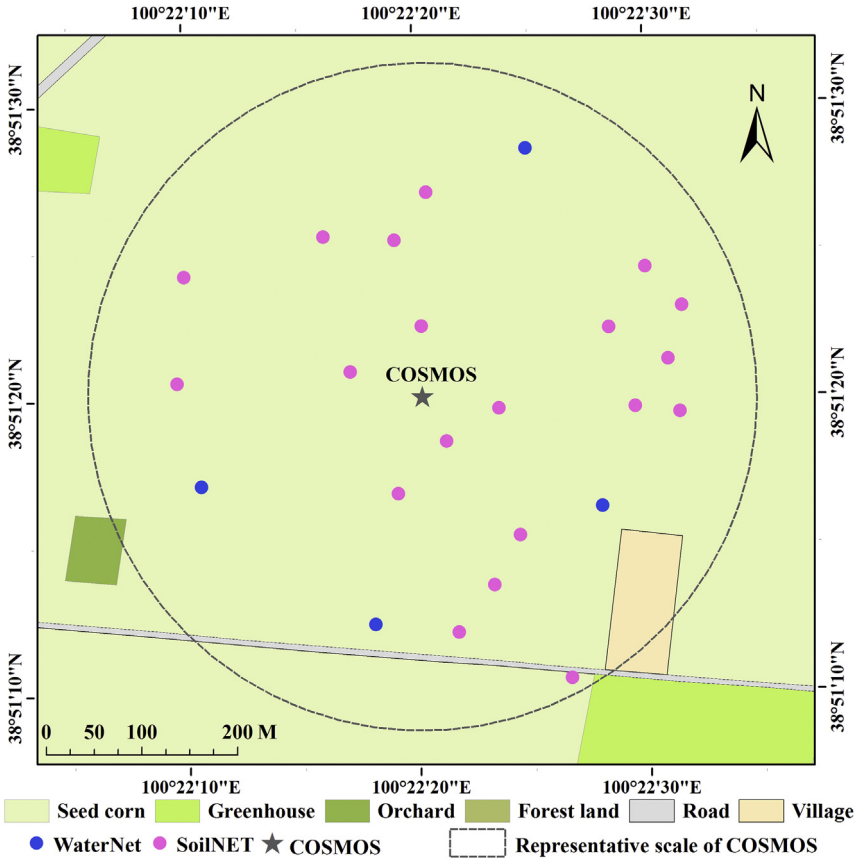

Fig. 3. The configurations of point-scale and footprint-scale measurements in the study area during an intensive observation period of HiWATER. The support scale of WaterNet and SoilNet is 0.1 m (regarded as zero or point scale), and the support scale of COSMOS is 700 m (regarded as macro-scale).

normal distribution is able to characterize the distribution of synthetic measurements. The synthetic measurements in this experiment can meet this criterion when the kurtosis of increments (decreasing progressively from 3.6084 to 2.8854) is significantly larger than that of samples (2.863) at small distances ($1 \leq d \leq 9$) then becomes smaller (from 2.7302 to 2.5771) when distances increase ($9 \leq d \leq 10$). These results prove that a method based on a normal distribution is not recommended in synthetic experiments.

The six methods were implemented at each simulation time to calculate the upscaling estimates. The results of the time series are illustrated in Fig. 4(a), and (b) zooms in on the results of the first 50 simulation times, where the gray dots represent the simulation measurements and the true macro-scale value is 10. In Fig. 4(b), the inadequacy of the BK method is evident, whereas the other results are indistinguishable.

To further compare the six methods, the MAE values between the upscaling results and the macro-scale values are shown in the first row of Table 1. According to Table 1, GSLPE produced the smallest MAE, indicating that this method had the highest precision. We again assert that despite being generated by a normal distribution-based field, the samples cannot be considered to have strict normal distributions, and it is better to apply a p-normal distribution to describe them. In the experiment based on normally distributed samples, LPE performed slightly better than LSE, and GSLPE performed the best because it also considers the spatial information. All of the methods exhibited similar MAE values, except BK and IDWLPE, which yielded the worst results, possibly because these two methods have difficulty capturing the heterogeneity in a region based on a normal random field. For IDWLPE, it is unreasonable to assume that the spatial correlation is only influenced by distance, and BK cannot correctly obtain the spatial correlation information because the study region is random.

Table 1 also shows the results of the robustness test. In this test, there was a 5% chance of each simulation measurement being approximately 5 times or 20% of its original value. The results are shown in the second and third rows of Table 1. Due to substantial robustness of the LPE and IDWLPE (Nyquist, 1980; Pennecchi and Callegaro, 2006), the MAE values barely increased. In contrast, the MAE values of the AA, BK and LSE methods significantly increased because these methods completely depend on minimizing the least square error and are therefore less robust. Compared to IDWLPE, GSLPE performed poorly and had a larger increment. This difference arose because although the iterative process of the GSLPE method was based on a p-normal distribution, the matrix of the spatial model B was deduced by ordinary kriging, which is less robust and provides unreasonable weights in the presence of considerable outliers in the measurements. Consequently, matrix B negatively affected the robustness during each iteration, and these errors accumulated and eventually produced poor estimates. IDWLPE had no requirements regarding the distribution characteristics of the measurements; thus, its performance was similar to that of the LPE method based on the robustness test.

The results of the stability test are illustrated in Fig. 5. Obviously, the estimates can be improved by increasing the number of simulation measurements used in all of the methods. The improvements were more significant for $s < 10$, and all of the methods produced stable results when $s > 20$. Notably, all of the MAE values fluctuated considerably when $s < 10$ and fluctuated much less when $s > 20$. This result confirmed that

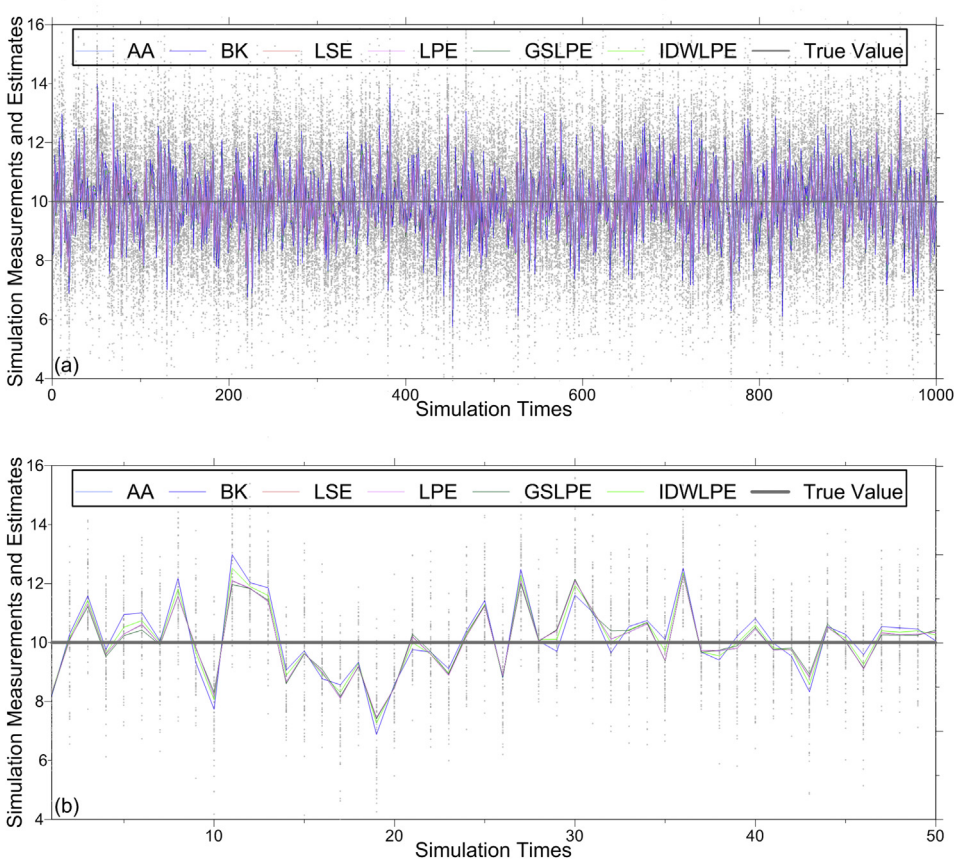

Fig. 4. Simulation measurements and estimates using the six upscaling methods (the simulation time is (a) $m = 1000$, (b) $m = 50$). The dots present the simulation measurements, the gray line is the mean of the true value, and the lines with different colors are the results generated by six upscaling methods. (For interpretation of the references to colour in this figure legend, the reader is referred to the web version of this article.)

Table 1
The upscaling results of the six methods in the synthetic experiment. The first row is the MAE (Mean Absolute Error) values between the upscaling results and the macro-scale values in the accuracy test, and the second and third rows show the MAE values and their changes in the robustness test where each measurement is randomly amplified or minimized according to a particular probability.

	AA	BK	LSE	LPE	GSLPE	IDWLPE
MAE	0.8738	0.9998	0.8727	0.8718	0.8670	0.9127
MAE (after modification)	1.2384	1.5837	1.2066	0.8779	1.065	0.9196
Increment	41.73%	58.40%	38.26%	0.70%	22.84%	0.76%

the reliability of the upscaling estimate could be increased by increasing the number of measurements. In addition, the disadvantages of BK indicated that a normal random field could have an adverse effect on the study of spatial correlation information.

In the real-world experiment, all point measurements were grouped according to the observation times, and each group of measurements was used to estimate the footprint-scale data (COSMOS data) at the same time using different upscaling methods. In addition to the six methods previously mentioned, a cokriging algorithm in conjunction with truncated power variogram (see Appendix, CKT is used below as an abbreviation) was also introduced in this experiment. A truncated power variogram model has the ability to represent multiscale overlapping random fields, e.g., the hydraulic data of a heterogeneous unconfined fluvial aquifer (Neuman et al., 2008) or the air permeability of an unsaturated fractured tuff (Neuman and Di Federico, 2003); therefore, this method is also applied to samples at diverse scales.

Fig. 6(a) shows the time series performances of the upscaling methods estimates and the COSMOS data from 2012-06-29 to 2012-08-30. A shorter period version of Fig. 6(a) is shown in Fig. 6(b), focusing on only two weeks. According to this figure, each upscaling method was found to simulate COSMOS data trends accurately, with small differences observed between the methods. The COSMOS data curves exhibited substantial variations, whereas the estimates of the point measurements fluctuated less. This result arose from the fact that the upscaling methods smoothed the differences between the multi-point values such that the estimates fell between the maximum and minimum point measurements.

In addition, the differences between the footprint-scale measurements and the estimates were significant, especially when the value dramatically changed. This phenomenon was partly caused by observational differences; specifically, the measurement techniques and retrieval models of the footprint data were not the same as those used to collect the point data, resulting in differences between the COSMOS data and the point measurements. Additionally, when rain or irrigation events occurred, the response speeds of point measurements varied according to their locations, resulting in estimates lagging behind the footprint data. Moreover, the upscaling methods still need to be improved, highlighting the inappropriateness of extrapolating multi-point measurements to a non-matched representative space. This difference consequently constitutes the representativeness errors between the footprint- and point-scale measurements.

Differences among the upscaling methods were also clear. At most of the observation times, the estimates of AA were the largest, followed by those of the LSE and BK. Moreover, compared to other methods, the p-normal-based methods produced much smaller estimates at a few observation times (as shown in the red boxes in Fig. 6(b)). This phenomenon may imply that some point measurements with lower values were assigned higher weights based on the LPE, resulting in smaller estimates.

The MAE values between the upscaling results and the COSMOS data observed from 2012-06-29 to 2012-08-30 are listed in the first row of Table 2. Among the first six methods, GSLPE and LPE produced the smallest MAE values, which correspond to higher precision, and the results of the AA and BK were the worst. The results highlight the advantage of p-normal-based upscaling methods and indicate that if the land surface heterogeneity is so complex that the spatial correlation information cannot be correctly captured by geostatistical methods, an overreliance on kriging may result in estimates that are no better than those obtained by a simple arithmetic average. IDWLPE performed slightly worse than LPE, demonstrating that the IDW method failed to understand the spatial correlation of the study area. The second and third row of Table 2 provide the MAE values between the upscaling results and the COSMOS data observed during the irrigation period from 2012-07-27

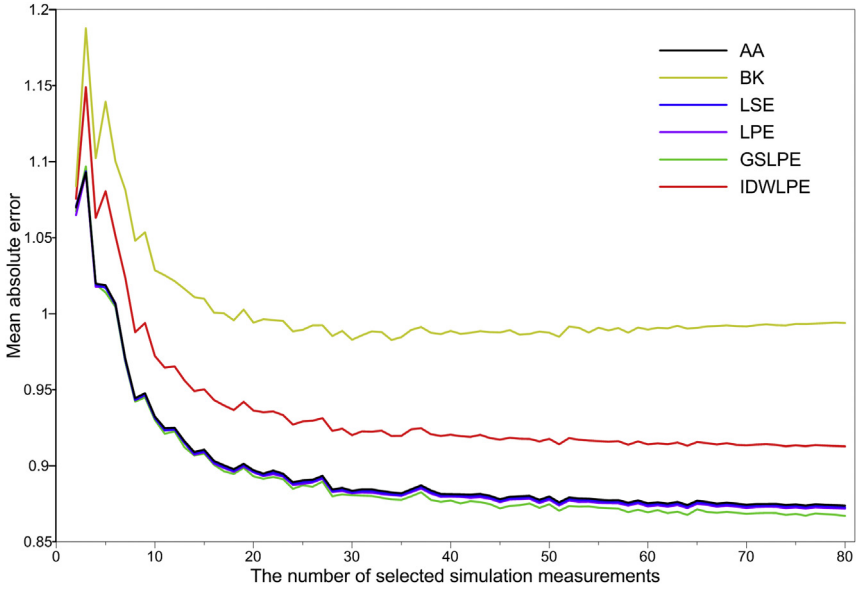

Fig. 5. Upscaling results using different numbers of simulations (The simulation time is $m = 1000$ and the repeat time for each select number is $N_r = 10$).

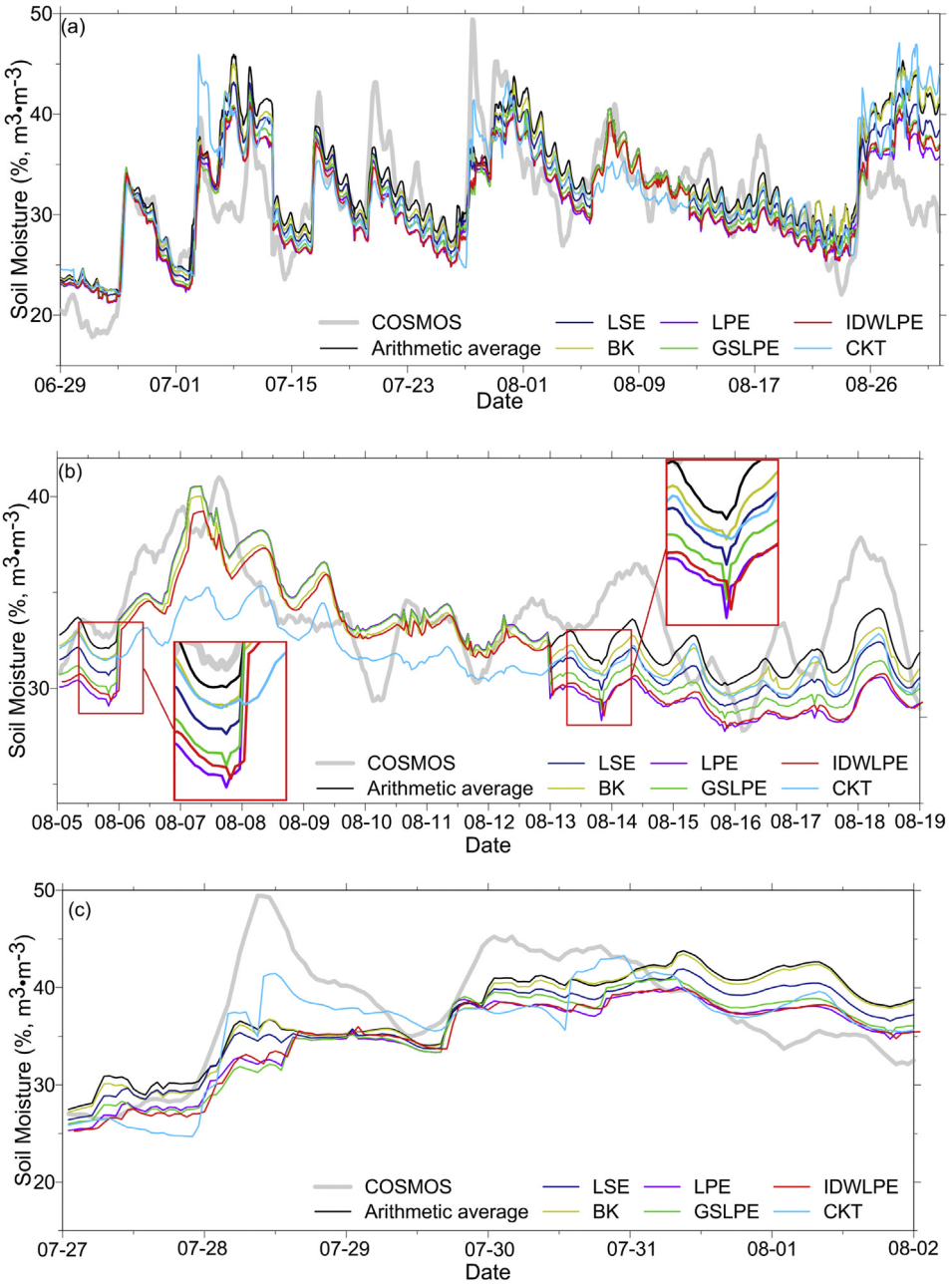

Fig. 6. The soil moisture time series of the upscaling method estimates and the COSMOS data (the bold gray line). (a) Time series from 2012-06-29 to 2012-08-30 (b) A shorter period of time series from 2012-08-05 to 2012-08-18 (c) Time series of the irrigation period from 2012-07-27 to 2012-08-02.

to 2012-08-02 (also see in Fig. 6(c)) and the increments that compared the MAE values during the irrigation period to those from 2012-06-29 to 2012-08-30. CKT performed poorly like AA and BK in the whole period, and became much better during the irrigation period. The change rate of CKT is as small as those of the methods based on the LPE. However, the reasons for the similar increments are different. Measurements during the irrigation period vary greatly, driving the increase in the MAE between estimates and "truth". As stated in the robustness test, LPE-based methods are more robust than others and produce smaller increments. Meanwhile, point-scale measurements vary with their locations during the irrigation period, e.g., measurements of soil moisture in irrigated areas are much bigger than those in unirrigated areas. Therefore, soil

Table 2
The MAE (Mean Absolute Error) value of the upscaling methods (Unit: $m^3\ m^{-3}$, %) in the real-world experiment. The first row is the MAE values between the upscaling results and the COSMOS measurements observed from 2012-06-29 to 2012-08-30, and the second and third rows show the MAE values and their changes during the irrigation period.

	AA	BK	LSE	LPE	GSLPE	IDWLPE	CKT
MAE	3.4708	3.4514	3.0737	2.9214	2.9423	2.9867	3.4695
MAE (irrigation period)	5.1936	5.1240	4.2994	3.6455	4.0208	3.7556	4.4755
Increment	49.63%	48.46%	39.87%	24.78%	36.65%	25.74%	28.99%

moisture measurements exhibit a heavy-tailed distribution, which is suitable for being processed by CKT and also leads to small increments.

4. Discussion and conclusions

This study included two independent experiments. The synthetic experiment included accuracy, stability and robustness tests, and the real-world experiment evaluated the comprehensive performance of the upscaling methods. The results indicated that the p-normal-based methods produced more precise macro-scale estimates compared to the estimates based on classic methods, which assume that the measurements are normally distributed and minimize the least square error to obtain maximum likelihood estimates.

The macro-scale "truth" was represented by the mean value of the random field in the synthetic experiment and by the COSMOS measurement in the real-world experiment. The former assumption is based on the mean homogeneity of the study region, and the latter is on the fact that the support scale of COSMOS measurement is much larger than the point-scale measurement. However, it is hard to conclude that the real-world measurements exactly represent the "truth" at their own support scale. Nonetheless, our study evaded this problem and all the macro- or point-scale measurements in the real-world experiment were regarded as the sum of the true value and random errors.

The effectiveness of all of the parameters in the upscaling methods can be described as follows. First, the experiments demonstrated the potentiality of the p parameter for improving the upscaling strategies. Equation (2) is commonly used to calculate the parameter p in the literature, and other methods are also recommended (Money et al., 1982; Pennecchi and Callegaro, 2006). One risk is that all the above calculations are empirical functions. This approximate function might result in an imprecise p parameter and, ultimately, poor upscaling estimates. Second, compared to the p parameter, variance may be more effective for upscaling methods. This conclusion is based on the phenomenon that AA and BK were always inferior to the other methods with respect to variance, and also based on the fact that the differences between AA and LES were substantially larger than those between the LSE and the LPE (compared with AA and LSE, LSE and LPE consider the variance and parameter p, respectively). This finding indicates that an upscaling method can be improved considerably if the variance is used. Third, the experiments showed that the LSE performed better than BK. However, the results do not demonstrate that variance is a more important factor than the spatial correlation information because in this study only simple geostatistical models (i.e., the exponential model, BK and ordinary kriging) were employed. Some advanced geostatistical models may more accurately capture spatial heterogeneity and result in better estimates. Therefore, a reasonable conclusion cannot be currently drawn regarding which factor – variance or spatial correlation information – is more important for upscaling strategy.

We introduced four statistical parameters in this upscaling study. However, the results did not present sufficient evidence to prove that a method requiring more parameters performs better. As mentioned above, the upscaling estimates are more sensitive to variance. This phenomenon implicates the asymmetries of functions among diverse parameters and a lack of metrics that can be used to evaluate different upscaling methods. We therefore believe that more tests based on simulated and observed data are needed to develop corresponding theoretical criteria.

The results indicated that the representativeness error, which denotes the deviation between the upscaling estimates and the corresponding "truth", is still difficult to remove in statistical upscaling studies. Based on the results of the stability test, we speculate that the representativeness error will always have a negative impact on the results, even if the total number of measurements approaches infinity. Additionally, in the real-world experiment, the measurement techniques and retrieval models of the soil moisture observations were entirely different between the footprint-scale and point-scale; therefore, the COSMOS data and upscaling estimates cannot be perfectly matched, even when the sampling of the point measurements and the statistical upscaling methods are perfect. In conclusion, the representativeness error can be quantified by statistical methods, but the best methods to control and understand this error remain undetermined. Other uncertainties, such as the error caused by incorrect parameter values or statistical model selection, may result in poor upscaling as well. These factors include the setting of the repeat time and the initial value of the algorithm, the choice of geostatistical model and parameters (Riva and Willmann, 2009; Nowak et al., 2010) and so on. Additional uncertainty arises from the imperfections in the observation techniques and the use of a numeric model to simulate dynamic processes. This study did not involve the related error analyses, but the fact that upscaling results can be affected by these uncertainties cannot be ignored.

Because each method focuses on different statistical parameters and exhibits distinct results in these numerical experiments, it is necessary to determine which upscaling method is more adequate according to the type of data being studied, especially when no prior statistical information is available. First, if the measurements have been strictly preprocessed and controlled and there are no outliers, methods based on the normal distribution hypothesis, such as multi-point arithmetic average, LSE or BK, are recommended because of their simplicity. In this situation, if the upscaling results are less than satisfactory, the LPE should be used because the measurements may not be normal, and the LPE can address more general samples by calculating the parameter p. Second, if the raw data are disorganized, LPE is a wise choice due to its robustness. Finally, if slight preprocessing has been performed and the spatial correlation information can be correctly captured, one can obtain a better estimate using GSLPE because it is robust enough to address outliers and can also improve the results by means of geostatistics. Note that the above conclusions are only based on the synthetic and real-world experiments conducted in this study.

This study focuses on extending upscaling methods with the p-normal distribution and exploring the possibility of upscaling multi-point measurements with spatial information and the LPE. Therefore, the optimal computation of the LPE and a thorough study to accurately capture the spatial correlation information, such as an anisotropy analysis, were not included. These efforts will enhance the estimation accuracy and deserve attention in the future.

Acknowledgments

The authors thank Prof. Alberto Guadagnini and the other two anonymous reviewers for their valuable comments and suggestions on the manuscript. This work was supported by the National Natural Science Foundation of China (91425303 and 91625103), the International Partnership Program of Chinese Academy of Sciences, Grant No. 131C11KYSB20160061 and the Cross-disciplinary Collaborative Teams Program for Science, Technology and Innovation of the Chinese Academy of Sciences.

Appendix

Multi-scale cokriging with truncated power variogram (CKT) refers to a method to estimate the value of a variable at desired scale. Consider the following system:

$$\begin{cases} \widehat{x} = \sum_{m=2}^{M} \sum_{i=1}^{N_m} \lambda_{m,i} x_{m,i}^{o} \\ \sum_{m=2}^{M} \sum_{i=1}^{N_m} \lambda_{m,i} = 1 \\ \sum_{m=2}^{M} \sum_{i=1}^{N_m} \lambda_{m,i} \gamma_{v,m}(c_{v,u} - c_{m,i}) - \xi = \gamma(c_0 - c_{v,u}), u = 1, \cdots, N_v, v = 2 \cdots, M \end{cases} \tag{A1}$$

where $x_{m,i}^{o}, m = 2 \cdots, M$ are the available measurements at scale s_m. If s_1 is the largest scale covering all the other scales, then the multiscale random fields are overlapping and $s_1 > s_2 > \cdots > s_M$. The subscript m presents the scale s_m; thus, $x_{m,i}^{o}$ is the ith measurement at scale s_m, N_m is the number of $x_{m,i}^{o}$, and $\lambda_{m,i}$ is the corresponding cokriging weight assigned to $x_{m,i}^{o}$.

In the last Equation in (A1), $c_{v,u}$ and $c_{m,i}$ are the geographic locations where $x_{u,v}^{o}$and $x_{m,i}^{o}$are measured, respectively. Semivariogram $\gamma_{v,m}(c_{v,u} - c_{m,i}) = \sigma_{min(v,m)}^2 - \frac{1}{2}(\sigma_v^2 + \sigma_m^2) + \tilde{\gamma}_{v,m}$, where σ^2 is the variance of a variable at the corresponding scale, and $\tilde{\gamma}_{v,m} = \int_{\frac{\mu}{s_v}}^{\frac{\mu}{s_m}} \gamma \frac{dn}{n}, \mu = constant$is the truncated power variogram.

In the synthetic and real-world experiments in this paper, there are only two different scales, resulting in $M = 2$. Equation (A1) is consequently reduced to a system of ordinary kriging as follows:

$$\begin{cases} \widehat{x} = \sum_{i=1}^{N} \lambda_i x_i^{o} \\ \sum_{i=1}^{N} \lambda_i = 1 \\ \sum_{i=1}^{N} \lambda_i \gamma(c_u - c_i) - \xi = \gamma(c_0 - c_u), u = 1, \cdots, N_v \end{cases} \tag{A2}$$

If $s_1 \gg s_2$, the semivariogram reduces to $\gamma(c_u - c_i) = \tilde{\gamma} = A_0 d^{2H}$, where $H$is the Hurst coefficient, $A_0 = A\Gamma(1 - 2H)/2H$(for exponential model, $0 < H \leq 0.5$) and $d$is the distance between geographic locations $c_u$and c_i.

The solution of system (A2) is based on the estimates of μ, $H$and A_0. Assuming that lag $a$and variances $\sigma_i^2,\ i = 1, 2$are available, μ, $H$and A_0can be found with the least square solutions of the following nonlinear system:

$$\begin{cases} \dfrac{2\mu s_2 H}{1 + 2H} = a \\ \dfrac{A(\mu s_2)^{2H}}{2H} = \sigma_2^2 \\ \dfrac{A\mu^{2H}\left(s_1^{2H} - s_2^{2H}\right)}{2H} = \sigma_1^2 - \sigma_2^2 \end{cases} \tag{A3}$$

In our study, we updated $a$with the experimental semivariogram at each time, and the variances $\sigma_1^2 = 0.04$and $\sigma_2^2 = 0.0137$.

The differences between LPE-based methods and CKT are clear. Compared with CKT, which performs better in a heavy-tailed distribution, the LPE-based methods are free of the probability distributions of the geophysical variables and produce more robust results if there are some outliers in the measurements. Furthermore, CKT specializes in capturing the multi-scale behavior of a geophysical variable ranging from the point scale to large windows, and its estimates are explicitly related to the magnitude of the scale (see Equation. (A1)). However, the LPE-based methods are only appropriate for point-scale measurements and the support scales of their estimates depend on how the available point measurements are sampled.

References

Atkinson, P.M., Tate, N.J., 2000. Spatial scale problems and geostatistical solutions: a review. Prof. Geogr. 519, 607–623.

Chen, J.M., Chen, B.S., Chang, W.S., 1994. Parameter estimation of linear systems with input-output noisy data: a generalized lp norm approach. Signal process.. 37, 345–356.

Famiglietti, J.S., Ryu, D., Berg, A.A., Rodell, M., Jackson, T.J., 2008. Field observations of soil moisture variability across scales. Water Resour. Res. 44.

Goovaerts, P., 1997. Geostatistics for Natural Resources Evaluation. Oxford university press, New York.

Gruber, A., Dorigo, W.A., Zwieback, S., Xaver, A., Wagner, W., 2013. Characterizing coarse-scale representativeness of in situ soil moisture measurements from the International Soil Moisture Network. Vadose Zone J. 12, 522–525.

Han, X., Jin, R., Li, X., Wang, S., 2014. Soil moisture estimation using cosmic-ray soil moisture sensing at heterogeneous Farmland. IEEE Geosci. Remote S 11, 1659–1663.

Jin, R., Li, X., Yan, B., Li, X., Luo, W., Ma, M., Guo, J., Kang, J., Zhu, Z., Zhao, S., 2014. A nested ecohydrological wireless sensor network for capturing the surface heterogeneity in the midstream areas of the Heihe River Basin, China. IEEE Geosci. Remote S 11, 2015–2019.

Kitanidis, P., 1986. Parameter uncertainty in estimation of spatial functions: Bayesian analysis. Water Resour. Res. 22, 499–507.

Krupiński, R., Purczyński, J., 2006. Approximated fast estimator for the shape parameter of generalized Gaussian distribution. Signal process.. 86, 205–211.

Kuruoğlu, Ercan E., Rayner, Peter J.W., Fitzgerald, William J., 1998. Least Lp-norm impulsive noise cancellation with polynomial filters. Signal process.. 69, 1–14.

Li, X., 2014. Characterization, controlling, and reduction of uncertainties in the modeling and observation of land-surface systems. Sci. Chin. Earth Sci. 57, 80–87.

Li, X., Cheng, G., Liu, S., Xiao, Q., Ma, M., Jin, R., Che, T., Liu, Q., Wang, W., Qi, Y., Wen, J., Li, H., Zhu, G., Guo, J., Ran, Y., Wang, S., Zhu, Z., Zhou, J., Hu, X., Xu, Z., 2013. Heihe watershed allied telemetry experimental research (HiWATER): scientific objectives and experimental design. B. Am. Meteorol. Soc. 94, 1145–1160.

Mandelbrot, B.B., 1967. How long is the coast of Britain? Science 156, 636–638.

Meerschman, E., Pirot, G., Mariethoz, G., Straubhaar, J., Van Meirvenne, M., Renard, P., 2013. A practical guide to performing multiple-point statistical simulations with the Direct Sampling algorithm. Comput. Geosci. 52, 307–324.

Molotch, N.P., Bales, R.C., 2005. Scaling snow observations from the point to the grid element: Implications for observation network design. Water Resour. Res. 41, 1–17.

Money, A.H., Affleck-Graves, J.F., Hart, M.L., Barr, G.D.I., 1982. The linear regression model: Lp norm estimation and the choice of p. Commun. Stat simul. C 11, 89–109.

Neuman, S.P., Di Federico, V., 2003. Multifaceted nature of hydrogeologic scaling and its interpretation. Rev. Geophys. 41 (3), 1014,. http://dx.doi.org/10.1029/2003RG000130.

Neuman, S.P., Riva, M., Guadagnini, A., 2008. On the geostatistical characterization of hierarchical media. Water Resour. Res. 44, 252–261. http://dx.doi.org/10.1029/2007WR006228.

Nowak, W., de Barros, F.P.J., Rubin, Y., 2010. Bayesian geostatistical design: task-driven optimal site investigation when the geostatistical model is uncertain. Water Resour. Res. 46 (3), W03535.

Nyquist, H., 1980. Recent Studies on Lp-norm Estimation. University of Umea, Sweden.

Panzeri, M., Riva, M., Guadagnini, A., Neuman, S.P., 2016. Theory and generation of conditional, scalable sub-Gaussian random fields. Water Resour. Res. 52, 1–16. http://dx.doi.org/10.1002/2015WR018348.

Pascal, F., Bombrun, L., Tourneret, J.-Y., Berthoumieu, Y., 2013. Parameter estimation for multivariate generalized Gaussian distributions. IEEE Trans. Sig. Process. 61, 5960–5971.

Pennecchi, F., Callegaro, L., 2006. Between the mean and the median: the Lp estimator. Metrologia 43, 213–219.

Renard, P., Allard, D., 2013. Connectivity metrics for subsurface flow and transport. Adv. Water Resour. 51, 168–196.

Riva, M., Willmann, M., 2009. Impact of log-transmissivity variogram structure on groundwater flow and transport predictions. Adv. Water Resour. 32, 1311–1322.

Riva, M., Neuman, S.P., Guadagnini, A., 2015. New scaling model for variables and increments with heavy-tailed distributions. Water Resour. Res. 51, 4623–4634. http://dx.doi.org/10.1002/2015WR016998.

Vereecken, H., Kasteel, R., Vanderborght, J., Harter, T., 2007. Upscaling hydraulic properties and soil water flow processes in heterogeneous soils. Vadose Zone J. 6, 1–28.

Wang, G., Gertner, G., Anderson, A.B., 2004. Up-scaling methods based on variability-weighting and simulation for inferring spatial information across scales. Int. J. Remote Sens. 25, 4961–4979.

Woodcock, C.E., Strahler, A.H., 1987. The factor of scale in remote sensing. Remote. Sens. Environ. 21, 311–332.

Yarlagadda, R., Bednar, J.B., Watt, T.L., 1985. Fast algorithms for lp-deconvolution. IEEE Trans. Acoust. Speech & Signal Process. 33, 174–182.

Zhu, Z., Tan, L., Gao, S., Jiao, Q., 2015. Observation on soil moisture of irrigation cropland by cosmic-ray probe. IEEE Geosci. Remote S 12, 472–476.